JACS
JOURNAL OF THE AMERICAN CHEMICAL SOCIETY

Communication

pubs.acs.org/JACS

Electron Doping in Bottom-Up Engineered Thermoelectric Nanomaterials through HCl-Mediated Ligand Displacement

Maria Ibáñez,[†] Rachel J. Korkosz,[‡] Zhishan Luo,[†] Pau Riba,[†] Doris Cadavid,[†] Silvia Ortega,[†] Andreu Cabot,*[,†,§] and Mercouri G. Kanatzidis*[,‡]

[†]Catalonia Energy Research Institute−IREC, Sant Adria del Besos, 08930 Barcelona, Spain

[‡]Department of Chemistry, Northwestern University, Evanston, Illinois 60208, United States

[§]Institució Catalana de Recerca i Estudis Avançats−ICREA, 08010 Barcelona, Spain

Supporting Information

ABSTRACT: A simple and effective method to introduce precise amounts of doping in nanomaterials produced from the bottom-up assembly of colloidal nanoparticles (NPs) is described. The procedure takes advantage of a ligand displacement step to incorporate controlled concentrations of halide ions while removing carboxylic acids from the NP surface. Upon consolidation of the NPs into dense pellets, halide ions diffuse within the crystal structure, doping the anion sublattice and achieving n-type electrical doping. Through the characterization of the thermoelectric properties of nanocrystalline PbS, we demonstrate this strategy to be effective to control charge transport properties on thermoelectric nanomaterials assembled from NP building blocks. This approach is subsequently extended to $PbTe_xSe_{1-x}$@PbS core−shell NPs, where a significant enhancement of the thermoelectric figure of merit is achieved.

The PbTe/Se-PbS bulk nanostructured systems are some of the most important thermoelectric materials under investigation.[1] Their high performance arises from their very low thermal conductivity and high power factor, translating into high thermoelectric figures of merit, $ZT = ((\sigma S^2)/\kappa)T$, where σ is the electrical conductivity, S is the thermopower, or Seebeck coefficient, κ is the thermal conductivity, and T is the temperature. These bulk materials are essentially biphasic where a second phase, e.g., PbS is on the nanoscale and embedded in a coherent (endotaxial) manner in the matrix phase, e.g., PbTe. This type of nanostructuring emerges from the nucleation and growth of one phase inside another in the solid state. Another type of nanostructuring can be envisioned in which colloidal nanocrystals of lead chalcogenides can be assembled and consolidated into bulk specimens. Colloidal NPs with tuned size, shape, crystal phase, and composition offer an exceptional platform for the precise and cost-effective engineering of functional bulk nanomaterials and thin films.[2] However, the presence of organic ligands at the NP surface and the extremely challenging introduction of controlled amounts of electrical dopants remain as the two main drawbacks of bottom-up assembled nanomaterials in technological applications.[3] While organic ligands limit charge transfer between NPs and between NPs and the media, the difficult control of the charge carrier concentration prevents the optimization of the material electronic and thermoelectric performance.

The exchange or displacement of surface organic ligands by short inorganic molecules represented a major step toward improving the charge transfer and transport properties in bottom-up assembled nanomaterials.[4] While inorganic ligands may volatilize or decompose upon thermal consolidation or stabilization,[5] frequently foreign ions incorporate to the NP lattice partially changing its composition and therefore its functional properties.[6] At first view, this is a drawback of inorganic ligand exchange strategies. However, when controlled, it can offer an excellent opportunity to dope and change the charge transport properties of the nanomaterials obtained from the bottom-up assembly of colloidal NPs.[7]

Herein, using thermoelectrically relevant PbQ (Q = S, Se, Te) NPs, we describe a surface treatment designed to both remove carboxylic acid ligands from NP surface and introduce controlled amounts of dopant thereby controlling their electrical properties. We demonstrate the suitability of the procedure by characterizing the thermoelectric properties of nanocrystalline PbS doped with controlled amounts of chlorine ions, which act as n-type dopants. We further demonstrate the potential of this process by preparing Cl-doped $PbTe_xSe_ySe_{1-x-y}$ nanocomposites with high thermoelectric performance from the assembly and consolidation of $PbTe_xSe_{1-x}$@PbS core−shell NPs.

PbS NPs were prepared by reacting lead oleate with elemental sulfur dissolved in oleylamine (Supporting Information, SI). Figure 1 displays a representative transmission electron microscopy (TEM) image of the 14 ± 1 nm, cube-shaped PbS NPs obtained by the above detailed procedure. Thermogravimetric analysis showed that even after purification by multiple precipitation/redispersion steps, significant amounts of organics (~6.7% in weight) remained at the NP surface (Figure SI1). We refer to the purified but untreated NPs as PbS-OA.

HCl was used to partially remove the OA from the NP surface and because chlorine is a commonly used n-type dopant in bulk PbS, usually introduced as $PbCl_2$.[8] Our hypothesis was that Cl^- would remain at the PbS NP surface and from there it would incorporate to the PbS anion sublattice during the bulk consolidation step. The displacement of OA by HCl was carried out by injecting controlled amounts of a 1.25 M HCl ethanol

Received: January 5, 2015
Published: March 11, 2015

DOI: 10.1021/jacs.5b00091
J. Am. Chem. Soc. 2015, 137, 4046−4049

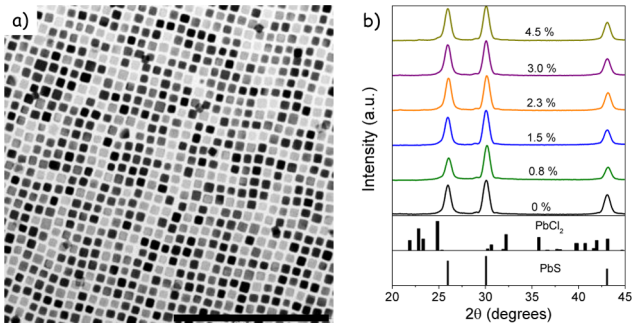

Figure 1. (a) TEM micrograph of 14 ± 1 nm, cube-shaped PbS NPs (scale bar = 100 nm). (b) XRD patterns of PbS NPs after ligand displacement with several HCl concentrations as noted.

solution in 1 g of PbS NPs dissolved in chloroform. The mixture was stirred at room temperature and in an argon filled glovebox for 1 h before purification by multiple precipitation/redispersion steps using anhydrous chloroform/methanol as a solvent/nonsolvent. We will refer to the samples obtained after this process as PbS-*x*%, *x* being the atomic concentration of Cl introduced. For HCl amounts up to 4.5%, PbS NPs remained soluble in relatively nonpolar solvents. Thermogravimetric analysis (Figure SI1) of the PbS-*x*% NPs treated with different HCl amounts clearly demonstrated the effectiveness of the HCl treatment to displace OA from the NP surface. It is important to highlight that all HCl concentrations presented in this work were calculated considering a 1.25 M solution of HCl in ethanol. Therefore, these numbers represent an upper limit on the HCl concentration, as HCl is highly volatile. In any case, no evidence of lead chloride was observed in the initial PbS-*x*% NPs from XRD analysis (Figure 1b).

As a reference, a PbS-0% sample, where all OA was displaced using NH_4SCN, was also produced. This sample was obtained by mixing 6 mL of a 130 mM NH_4SCN solution in methanol with 1 g of PbS NPs suspended in anhydrous chloroform.[5a] NPs were then purified using chloroform and methanol to remove free carboxylic acid and excess NH_4SCN, respectively.

Untreated and HCl- and NH_4SCN-treated PbS NPs were dried and annealed under Ar flow at 400 °C for 1 h to remove the remaining organic surfacants and to promote the insertion of Cl^- ions into the anion sublattice of the bulk nanocomposite. The obtained nanopowders were subsequently consolidated in a hot press system (SI) into 10 mm in diameter and ∼1 mm thick disk-shaped pellets at 40 MPa and 400 °C in an inert atmosphere. PbS-OA and PbS-*x*% pellets with relative densities of 85% and above 90%, respectively, were finally obtained. During these two thermal processes, crystal domains grew from the initial 14 nm to ∼50 nm for the PbS-OA and ∼55 nm for PbS-*x*% as calculated from the fitting of the XRD patterns using Scherrer eq (Figure SI2). Moreover, in the PbS-9.0% sample, peaks corresponding to the $PbCl_2$ phase were identified in the XRD patterns obtained after the annealing processes (Figure SI2).

Figure 2 shows the electrical conductivity and Seebeck coefficient of the consolidated nanocrystalline PbS pellets obtained from PbS-OA NPs and PbS-*x*% NPs with 0% ≤ *x* ≤ 4.5%. PbS-OA samples (undoped) were characterized by relatively low electrical conductivities with a characteristic step increase of the conductivity above 450 K. This step change of the electrical conductivity was accompanied by a simultaneous step change of the Seebeck coefficient that included a sign inversion at around 450 K, from positive to negative values. The low electrical

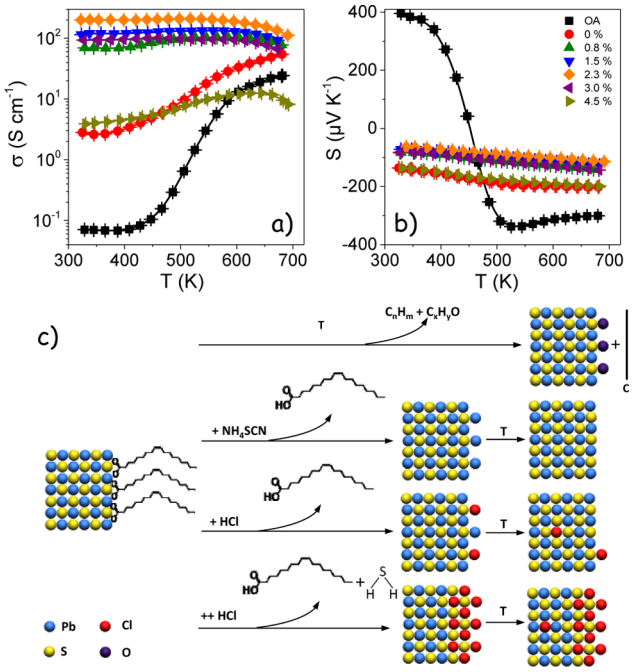

Figure 2. Electrical conductivity (a) and Seebeck coefficient (b) of nanocrystalline PbS obtained from the bottom-up assembly of PbS-OA NPs and PbS-*x*% NPs with 0% < *x* < 9% as noted in the legend. (c) Scheme of the HCl-based doping strategy.

conductivity at low temperature and the electrical conductivity and Seebeck coefficient step changes above 400 K, suggesting a low concentration of charge carriers at room temperature and a thermal activation of a relatively large concentration of negative charge carriers above 400 K.

The removal of organic ligands using NH_4SCN, PbS-0%, resulted in a strong increase of the electrical conductivity in the low temperature range (Figure 2a). The step change at 450 K observed in PbS-OA was preserved, and a monotonous increase of the electrical conductivity was measured up to 700 K. However, a negative Seebeck coefficient, but smaller in absolute value to that obtained for PbS-OA, was measured in the whole temperature range evaluated (Figure 2b). These results confirm the n-type doping as a result of the NH_4SCN treatment. We associate this increase of the electrical conductivity and the shift toward negative Seebeck coefficients with the removal of S from PbS NPs during the thermal treatment. This was not observed in the PbS-OA samples because of the protection given by the surface organic/carbon layer toward S removal and by a possible surface oxide layer formed from the decomposition of the OA carboxylic group during annealing.[9] Nevertheless, no PbO phase was identified from XRD analysis.

Pellets produced from HCl-treated NPs were characterized by significantly higher electrical conductivities. Moreover, the electrical conductivities increased with the amount of Cl introduced, up to 2.3%. Above this concentration, a decrease of electrical conductivity, associated with the formation of a $PbCl_2$ secondary phase (Figure SI2), was observed. All PbS-*x*% nanomaterial samples showed negative Seebeck coefficients with monotonically decreasing absolute values as expected for increasing degree of n-type doping (Figure 2b). However, the Seebeck coefficient absolute values obtained for the PbS-*x*% (*x* > 0) samples were significantly lower than those obtained for PbS-OA and PbS-0%, which indicates a higher carrier concentration due to successful doping with the Cl anions.

DOI: 10.1021/jacs.5b00091
J. Am. Chem. Soc. 2015, 137, 4046−4049

From these results, we conclude that HCl is able to displace oleic acid by breaking the lead oleate Pb−O bonds stabilizing the PbS NP surface. As a result of this reaction, free OA is released to the solution and chlorine ions react with surface Pb cations to form $PbCl_2$. Additionally, small amounts of sulfide ions may be removed by the formation of H_2S (Figure 2c). The data clearly indicate that during the thermal treatment, the chloride ions diffuse within PbS and incorporate to the anion sublattice, acting as electron donors.

We note that the thermal treatments also introduce a small stoichiometry imbalance in PbS-*x*% due to partial sulfide removal. However, electrical conductivities obtained with the HCl treatment were much higher than with the NH_4SCN treatment, pointing toward a much stronger doping influence of the chlorine ion. Furthermore, the doping level could be controlled by adjusting the amount of HCl introduced.

To further differentiate the influence of the two treatments, a second set of HCl-treated samples was produced by subsequently treating the samples first with the appropriate amount of HCl and subsequently with an excess of NH_4SCN to remove all remaining OA. The thermoelectric properties of this second set of samples did not substantially differ from those obtained from materials treated just with HCl (Figure SI3).

These results overall demonstrate the strong influence of the surface treatment with hydrogen halides on the transport properties of PbS nanocrystalline materials and suggests a key role of such introduced halide ions as n-type dopants (Figure 2c). While PbS provided us with a simple system to demonstrate the potential of the developed procedure to introduce controlled amounts of dopants, in order to prove the potential of this strategy for achieving a high thermoelectric figure of merit for the bottom-up assembled nanocrystalline materials, we prepared new nanomaterial based on $PbTe_xSe_{1-x}$@PbS core−shell NPs and applied the same doping strategy.

$PbTe_xSe_{1-x}$@PbS core−shell NPs were produced by consecutive reactions of lead oleate with chalcogens following a combination of the methods developed by Quan et al.[10] to produce $PbTe_xSe_{1-x}$ cores and ourselves to produce PbTe@PbS core−shell NPs (SI).[11] Figure 3 displays representative TEM micrographs of the cube-shaped $PbTe_xSe_{1-x}$ cores and the final $PbTe_xSe_{1-x}$@PbS core−shell NPs produced. The average size of the cores and core−shell NPs was 9 ± 1 and 14 ± 1 nm, respectively. The composition of the core−shell NPs further used in this work was $(PbTe_{0.2}Se_{0.8})_{0.47}@(PbS)_{0.53}$. Following the same procedure described above, chlorine was introduced within the lead chalcogenide lattice using HCl to displace OA from the surface of the NPs. After the HCl treatment, the $PbTe_{0.2}Se_{0.8}$@PbS NPs were purified, dried, and annealed at 400 °C for 1 h. The obtained nanopowder was consolidated into 10 mm pellets at 40 MPa and 450 °C using spark plasma sintering (SPS). Densities around 85% and 93% were systematically obtained for $PbTe_{0.1}Se_{0.4}S_{0.5}$-OA and $PbTe_{0.1}Se_{0.4}S_{0.5}$-Cl pellets, respectively.

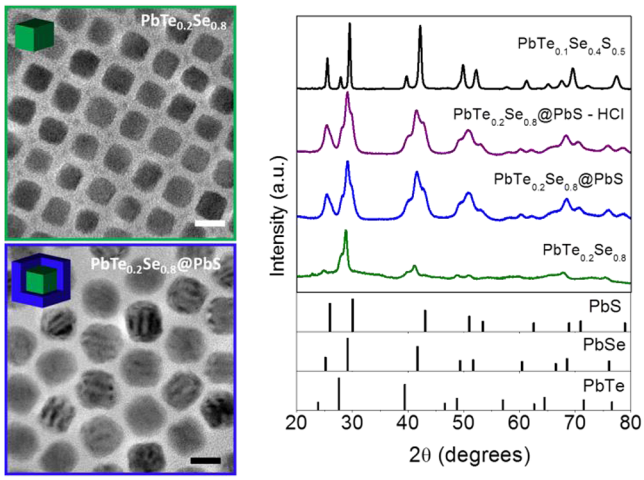

Figure 3. TEM micrographs of $PbTe_{0.2}Se_{0.8}$ and $PbTe_{0.2}Se_{0.8}$@PbS NPs (scale bar = 10 nm) and XRD patterns of $PbTe_{0.2}Se_{0.8}$ NPs, $PbTe_{0.2}Se_{0.8}$@PbS NPs before and after HCl ligand exchange, and $PbTe_{0.1}Se_{0.4}S_{0.5}$ nanomaterial obtained after SPS.

Figure 3 displays the XRD pattern of the initial $PbTe_{0.2}Se_{0.8}$ cores, the $(PbTe_{0.2}Se_{0.8})_{0.47}@(PbS)_{0.53}$ core−shell NPs, and the $PbTe_{0.1}Se_{0.4}S_{0.5}$ bulk nanomaterial obtained after SPS. XRD analysis shows the initial $PbTe_{0.2}Se_{0.8}$ cores to be probably a core−shell NP in themselves. After SPS processing a PbTe phase was clearly identified from the XRD pattern. However, the PbSe from the core was found forming a PbSeS alloy with the PbS from the shell.

Figure 4 shows the electrical conductivity, Seebeck coefficient, thermal conductivity, and final figure of merit of two $PbTe_{0.1}Se_{0.4}S_{0.5}$ bulk nanocrystalline materials obtained from the bottom-up assembly of $(PbTe_{0.2}Se_{0.8})_{0.47}@(PbS)_{0.53}$ core−shell NPs with and without HCl treatment (2.3%). A dependence of the electrical conductivity and the Seebeck coefficient with the temperature similar to that observed for PbS, including a step change of electrical conductivity at around 500 K, was obtained. A sign inversion of the Seebeck coefficient at around 350 K, was observed for the $PbTe_{0.1}Se_{0.4}S_{0.5}$-OA sample. Upon organic removal with 2.3% HCl, close to 4 orders of magnitude higher electrical conductivities were obtained, Figure 4a. The absolute value of the negative Seebeck coefficient obtained for the $PbTe_{0.1}Se_{0.4}S_{0.5}$-Cl sample increased with temperature, reaching similar values as those obtained from $PbTe_{0.1}Se_{0.4}S_{0.5}$-OA, up to ~180 μV K^{-1}, Figure 4b.

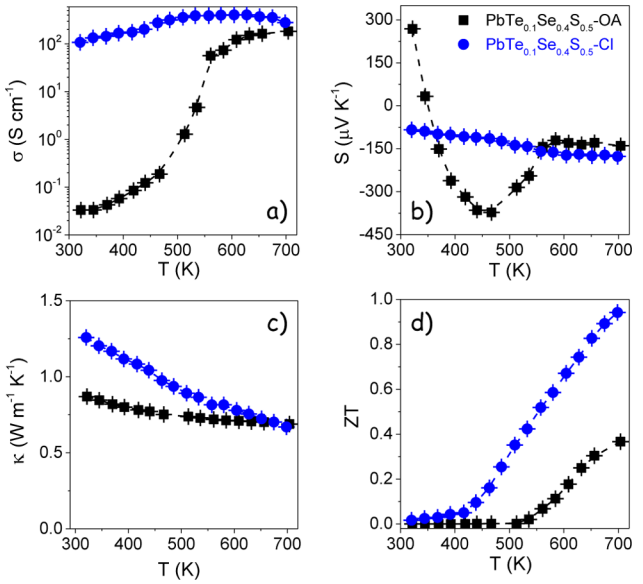

Figure 4. Electrical conductivity (a), Seebeck coefficient (b), thermal conductivity (c), and thermoelectric figure of merit (d) of nanocrystalline $PbTe_xSe_yS_{1-x-y}$ obtained from the bottom-up assembly of $PbTe_xSe_{1-x}$@PbS core−shell NPs with and without 2.3% HCl addition.

DOI: 10.1021/jacs.5b00091
J. Am. Chem. Soc. 2015, 137, 4046−4049

Relatively low thermal conductivities were obtained for both types of nanocrystalline materials, Figure 4c. The low thermal conductivities (~0.7 W/mK) indicate an efficient scattering of phonons at the large density of point defects and interfaces in these nanocrystalline alloy composites. Lower thermal conductivities were measured for the $PbTe_{0.1}Se_{0.4}S_{0.5}$-OA sample, which may be related to residual carbon at the grain boundaries provided from the decomposition of OA and to the slightly smaller crystal domains when compared with $PbTe_{0.1}Se_{0.4}S_{0.5}$-Cl.

Finally, a 2.6-fold increase in the thermoelectric figure of merit, up to ZT = 0.94, was obtained for the $PbTe_{0.1}Se_{0.4}S_{0.5}$-Cl nanocrystalline material compared with the $PbTe_{0.1}Se_{0.4}S_{0.5}$-OA sample, Figure 4d. The high ZT values obtained are comparable to the best figures of merit measured for bulk PbSe-PbS systems obtained by using long thermal processes (t > 60 h) at high temperatures ($T \approx 1150$ °C).[12]

In summary, we detailed a NP surface treatment procedure both to displace organic ligands and to introduce controlled amounts of halide ions as n-type doping elements. The convenience of the process was established with PbS, and the potential of the procedure was demonstrated with $PbTe_xSe_{1-x}$@PbS core−shell NPs, which possess ZTs comparable to bulk n-type PbTe. We believe this strategy to be generally applicable to all NPs stabilized with carboxylic acids and being potentially dopable by halide anions.

■ ASSOCIATED CONTENT

Supporting Information

Additional experimental and material characterization details. This material is available free of charge via the Internet at http://pubs.acs.org.

■ AUTHOR INFORMATION

Corresponding Authors

*acabot@irec.cat

*m-kanatzidis@northwestern.edu

Notes

The authors declare no competing financial interest.

■ ACKNOWLEDGMENTS

At IREC, work was supported by European Regional Development Funds and the Framework 7 program under project UNION (FP7-NMP 310250). M.I. and S.O. thank AGAUR for their Beatriu i Pinós postdoctoral grant and the PhD grant, respectively. At Northwestern, work was supported by the Revolutionary Materials for Solid State Energy Conversion, an Energy Frontier Research Center funded by the U.S. Department of Energy, Office of Science, and Office of Basic Energy Sciences under Award Number DE-SC0001054.

■ REFERENCES

(1) (a) Wu, H. J.; Zhao, L. D.; Zheng, F. S.; Wu, D.; Pei, Y. L.; Tong, X.; Kanatzidis, M. G.; He, J. Q. *Nat. Commun.* **2014**, *5*, 4515. (b) Girard, S. N.; He, J.; Zhou, X.; Shoemaker, D.; Jaworski, C. M.; Uher, C.; Dravid, V. P.; Heremans, J. P.; Kanatzidis, M. G. *J. Am. Chem. Soc.* **2011**, *133*, 16588−16597. (c) Heremans, J. P.; Jovovic, V.; Toberer, E. S.; Saramat, A.; Kurosaki, K.; Charoenphakdee, A.; Yamanaka, S.; Snyder, G. J. *Science* **2008**, *321*, 554−557. (d) Aminorroaya Yamini, S.; Wang, H.; Gibbs, Z. M.; Pei, Y.; Mitchell, D. R. G.; Dou, S. X.; Snyder, G. J. *Acta Mater.* **2014**, *80*, 365−372.

(2) (a) Ibáñez, M.; Cabot, A. *Science* **2013**, *340*, 935−936. (b) Talapin, D. V.; Lee, J.-S.; Kovalenko, M. V.; Shevchenko, E. V. *Chem. Rev.* **2010**, *110*, 389−458. (c) Yin, Y.; Alivisatos, A. P. *Nature* **2005**, *437*, 664−670.

(3) (a) Mocatta, D.; Cohen, G.; Schattner, J.; Millo, O.; Rabani, E.; Banin, U. *Science* **2011**, *332*, 77−81. (b) Erwin, S. C.; Zu, L.; Haftel, M. I.; Efros, A. L.; Kennedy, T. A.; Norris, D. J. *Nature* **2005**, *436*, 91−94.

(4) (a) Kovalenko, M. V.; Scheele, M.; Talapin, D. V. *Science* **2009**, *324*, 1417−1420. (b) Dong, A.; Ye, X.; Chen, J.; Kang, Y.; Gordon, T.; Kikkawa, J. M.; Murray, C. B. *J. Am. Chem. Soc.* **2010**, *133*, 998−1006.

(5) (a) Fafarman, A. T.; Koh, W.-k.; Diroll, B. T.; Kim, D. K.; Ko, D.-K.; Oh, S. J.; Ye, X.; Doan-Nguyen, V.; Crump, M. R.; Reifsnyder, D. C.; Murray, C. B.; Kagan, C. R. *J. Am. Chem. Soc.* **2011**, *133*, 15753−15761. (b) Carrete, A.; Shavel, A.; Fontané, X.; Montserrat, J.; Fan, J.; Ibáñez, M.; Saucedo, E.; Pérez-Rodríguez, A.; Cabot, A. *J. Am. Chem. Soc.* **2013**, *135*, 15982−15985.

(6) Kovalenko, M. V.; Spokoyny, B.; Lee, J.-S.; Scheele, M.; Weber, A.; Perera, S.; Landry, D.; Talapin, D. V. *J. Am. Chem. Soc.* **2010**, *132*, 6686−6695.

(7) (a) Buonsanti, R.; Milliron, D. J. *Chem. Mater.* **2013**, *25*, 1305−1317. (b) Yakunin, S.; Dirin, D. N.; Protesescu, L.; Sytnyk, M.; Tollabimazraehno, S.; Humer, M.; Hackl, F.; Fromherz, T.; Bodnarchuk, M. I.; Kovalenko, M. V.; Heiss, W. *ACS Nano* **2014**, *8*, 12883−12894.

(8) (a) Androulakis, J.; Chung, D.-Y.; Su, X.; Zhang, L.; Uher, C.; Hasapis, T.; Hatzikraniotis, E.; Paraskevopoulos, K.; Kanatzidis, M. *Phys. Rev. B* **2011**, *84*, 155207. (b) Zhao, L.-D.; Lo, S.-H.; He, J.; Li, H.; Biswas, K.; Androulakis, J.; Wu, C.-I.; Hogan, T. P.; Chung, D.-Y.; Dravid, V. P.; Kanatzidis, M. G. *J. Am. Chem. Soc.* **2011**, *133*, 20476−20487.

(9) (a) Marks, B. M.; Howard, H. C. *J. Phys. Chem.* **1927**, *32*, 1040−1048. (b) Zherebetskyy, D.; Scheele, M.; Zhang, Y.; Bronstein, N.; Thompson, C.; Britt, D.; Salmeron, M.; Alivisatos, P.; Wang, L.-W. *Science* **2014**, *344*, 1380−1384. (c) Hyeon, T. *Chemm. Comm.* **2003**, 927−934.

(10) Quan, Z.; Luo, Z.; Loc, W. S.; Zhang, J.; Wang, Y.; Yang, K.; Porter, N.; Lin, J.; Wang, H.; Fang, J. *J. Am. Chem. Soc.* **2011**, *133*, 17590−17593.

(11) Ibáñez, M.; Zamani, R.; Gorsse, S.; Fan, J.; Ortega, S.; Cadavid, D.; Morante, J. R.; Arbiol, J.; Cabot, A. *ACS Nano* **2013**, *7*, 2573−2586.

(12) Androulakis, J.; Todorov, I.; He, J.; Chung, D.-Y.; Dravid, V.; Kanatzidis, M. *J. Am. Chem. Soc.* **2011**, *133*, 10920−10927.

DOI: 10.1021/jacs.5b00091
J. Am. Chem. Soc. 2015, 137, 4046−4049